

A Quantitative Evaluation of 3D Soft Tissue Prediction in Maxillofacial Surgery Planning

S. Zachow^{1*}, Th. Hierl², and B. Erdmann¹

¹ Zuse-Institute Berlin (ZIB)

² Department of Oral-Maxillofacial, Plastic & Reconstructive Surgery
University Hospital Leipzig, Germany

Abstract. The aim of our work is to provide maxillofacial surgeons with an integrated osteotomy planning system for complex bone relocations, facilitating a preoperative assessment of functional as well as aesthetic rehabilitation. On this account we try to establish a robust modeling approach based on a histomechanical soft tissue model that reliably predicts the postoperative facial appearance. For two patients with distinct midfacial hypoplasia a maxillary advancement has been exactly reproduced from postoperative CT data, and applied to a 3D planning model derived from preoperative CT data. The resulting tissue deformations have been computed with a finite element approximation on a tetrahedral discretization of the patients' soft tissue. Isotropic, homogeneous as well as inhomogeneous tissue models are investigated. The simulation results are quantitatively compared to the true postoperative outcome.

1 Motivation

In maxillofacial surgery, physicians are often faced with complex bone relocations due to skeletal dysmorphisms, that require extensive preoperative planning. Especially for severe dysgnathia or hemifacial microsomia, where multiple bone segments are to be mobilized and relocated simultaneously and in relation to each other, the aesthetic outcome, i.e. the postoperative facial appearance, at present can only be estimated by surgical experience. On this account, a preoperative planning of different therapeutic strategies under consideration of soft tissue deformation, based on patient specific 3D models, tissue mechanics and a robust and reliable numerical simulation is highly desired by maxillofacial surgeons [1]. The determination, verification and optimization of representative histomechanical soft tissue models for surgery planning and simulating is subject of current research [2,3].

2 Patients and Data

For two patients with distinct midfacial hypoplasia and class III dysgnathia, as shown in Figure 1, corrective maxillofacial surgery has been performed. In both cases the designated therapy was a midfacial distraction osteogenesis using the Leipzig retention plate technique [4]. A thorough preoperative planning and preparation is indispensable.

* zachow@zib.de – www.zib.de/visual/projects/cas



Fig. 1. Patients with midfacial hypoplasia and ANGLE class III dysgnathia

The complete therapy planning, including osteotomy selection, bone cutting, maxillary advancement, assessment of the dental occlusion as well as 3D soft tissue prediction was performed with our surgery planning and simulation environment [5,6,7]. In both cases, approximately two weeks after removal of the retention system, a second CT was acquired for postoperative follow-up (Fig. 2). For the pre- and the postoperative scans the same imaging systems, a Siemens Somatom Plus 4, resp. a Siemens Volume Zoom have been used, with special attention to a minimum dose distribution [8]. The scan parameters were equally chosen, solely the field of view was slightly different.

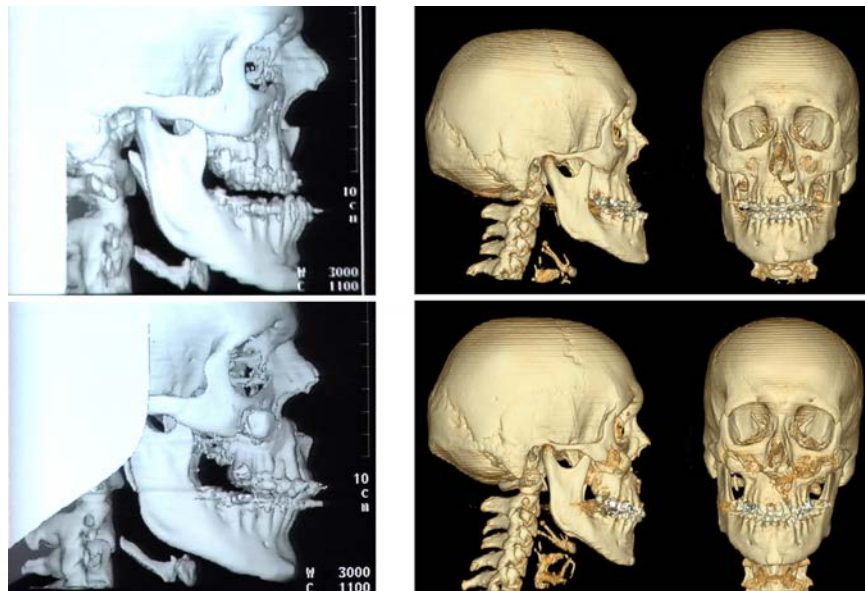


Fig. 2. top) preoperative, bottom) postoperative CT-data for the 2 patients in Fig. 1

3 Material and Methods

On the basis of pre- and postoperative CT data, the performed surgery was accurately reproduced with regard to the exact bone relocation, and the resulting soft tissue deformation was simulated to compare the prediction with the true postoperative outcome. Thus, we are able to assess the quality of our simulation, and to determine suitable histomechanic parameters for improving our modeling approach [7].

3.1 Pre- and Postoperative 3D Model

To get a comparable reconstruction of bone with regard to thickness and volume, a suitable segmentation threshold has to be identified in both data sets. These values were determined by comparison of the volume of the hyoid. In one case a threshold of 195 HOUNSFIELD units (HU) has been chosen for the preoperative data set with a voxel size of $0.41 \times 0.41 \times 1$ mm, resulting in a volume of 1.471 cm^3 . For the postoperative data a threshold of 180 HU lead to a comparable volume of 1.473 cm^3 with a voxel size of $0.44 \times 0.44 \times 1$ mm. The reconstruction for the second patient has been performed accordingly. In a subsequent segmentation step, metal artifacts were eliminated and thin bone structures, that got lost due to partial volume effects, were reconstructed.

3.2 Alignment of the Pre- and the Postoperative Skull Model

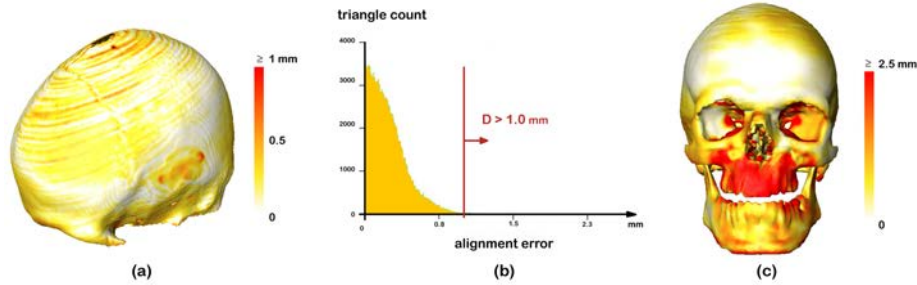


Fig. 3. a) color coded alignment error for the neurocranium, b) histogram of the deviation, c) color coded deviation on top of the preoperative skull surface

After 3D surface reconstruction the pre- and the postoperative skull models were registered using an iterative closest point (ICP) algorithm [9]. The alignment has been performed for the skull base only, because this region wasn't affected by the operation (Fig. 3 a). The corresponding regions consisted of approx. 400 000 triangles (200 000 vertices) each. The two-sided HAUSDORFF distance $D_2 = \text{argmax}(d(S_1, S_2), d(S_2, S_1))$ has been minimized, with the postoperative model as a reference [10]. The iterative alignment stopped with a relative deviation of the mean squared distance between two iteration steps below 10^{-6} . The mean distances between the aligned surfaces were 0.24

and $0,19\text{mm}$ respectively, with a standard deviation of approx. $0,20\text{mm}$. For only $0,5\%$ of the surface the deviation was above 1mm (Fig. 3 b). The resulting rigid transformation was finally applied to the entire preoperative model (Fig. 3 c), giving a mean distance of $1,2\text{mm}$ with a standard deviation of $1,5\text{mm}$ and a median of $0,68\text{mm}$. The maximum deviation for the relocated maxilla was $15,58\text{mm}$ in one case, and $11,2\text{mm}$ in the other case. Mobile bones like the mandible, the hyoid and the spine exhibited a maximum deviation of up to 5mm .

3.3 Osteotomy and Bone Relocation

For being able to compare the soft tissue prediction with the postoperative result, the osteotomy as well as the maxillary advancement must be reproduced as accurate as possible. The osteotomy lines were precisely traced on top of the preoperative bone surface, guided by the color coded deviation of the aligned pre- and postoperative skull, with an appropriately chosen color map (Fig. 3 c). Afterwards, the maxillary regions of the preoperative models have been mobilized for both patient models [6].

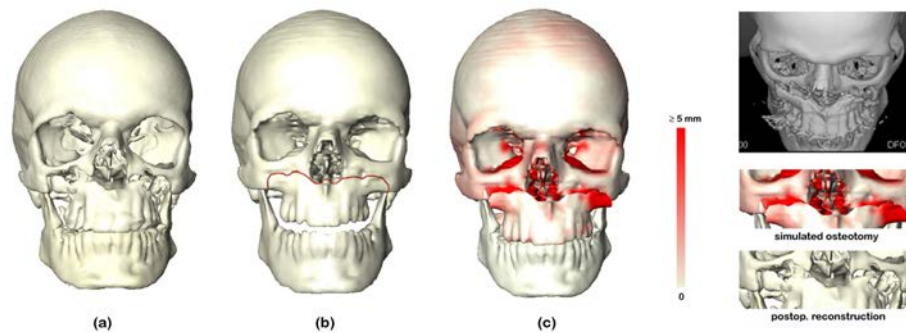


Fig. 4. a) postoperative skull reconstruction, b) osteotomized preoperative model, c) maxillary advancement and mandible rotation for the preop. model according to the postop. situation with color coded deviation for the entire skull model

For the maxillary advancement suitable corresponding landmarks were chosen, i.e. prominent points on and between the teeth, as well as the *spina nasalis anterior*, for instance. In a similar manner anatomical landmarks for the mandible have been specified to compensate the different positions within the pre- and the postoperative scans. A landmark based rigid transformation of the maxilla and the mandible finally lead to a configuration that accurately mimics the postoperative situation (Fig. 4). Due to a less accurate segmentation, there are still some discrepancies at the orbita walls of the postoperative model that can admittedly be neglected. However, for the patient model depicted in Fig. 4, an obvious difference can be seen at the infra-orbital rim, where a piece of bone fractured during surgery. This area, having no counterpart on the preoperative model, must remain in place for the simulation. For all other regions the deviation between modified pre- and postoperative model was below 1mm .

3.4 Soft Tissue Prediction

On the basis of the modified skull models, the resulting soft tissue deformation has been computed via a finite-element approach on an unstructured tetrahedral grid of the entire head. Soft tissue, is modeled as isotropic and linear elastic St.-Venant–Kirchhoff material, having only two independent elastic constants, i.e. POISSON’s ratio ν and YOUNG’s modulus E . Strains are described with the linearized CAUCHY strain tensor $\boldsymbol{\varepsilon}(\mathbf{u}) = \frac{1}{2}(\nabla\mathbf{u} + (\nabla\mathbf{u})^T)$ [5].

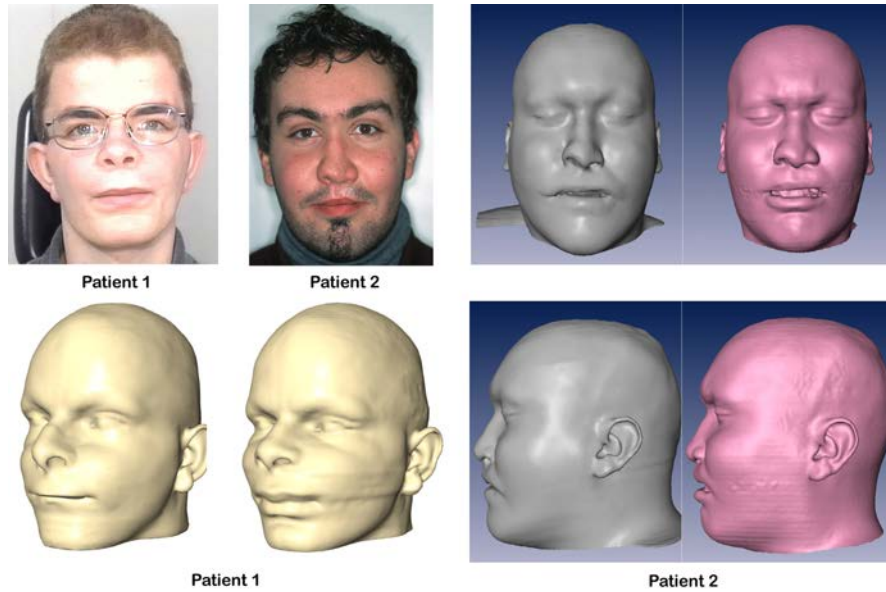


Fig. 5. Postoperative results and comparison with the prediction for the two patients. Bottom and right: left \rightarrow prediction, right \rightarrow postop. result

3.5 Quantitative Assessment of the Simulation Results

In a first investigation, where a *homogeneous*, almost incompressible tissue model was assumed, the value for POISSON’s ratio ν was varied within the range of $[0.3 \dots 0.5]$ [7], and the two-sided HAUSDORFF distance $D_2(\nu)$ between the predicted and the postoperative facial skin surface has been computed. Since the best correspondence between the simulation and the postoperative result was found with decreasing values $\nu \rightarrow 0.3$, we extended the range to $[0.0 \dots 0.5]$ (Tab. 1). In that case a minimum was found for $\nu = 0$, being definitely in contradiction to the assumption of incompressibility. The inspection of the soft tissue’s volume showed that the patient significantly lost weight due to his reduced chewing capabilities, so a model with higher compressibility partially compensated this difference. For the other patient a best correspondence was achieved for $0.43 < \nu < 0.45$ (Fig. 6), that nicely coincides with the literature values [11,12].

Table 1. Parameter study: Deviation between predicted skin surface and postoperative result for a *homogeneous* tissue model with varying POISSON ratio for two patients

ν	mean [mm]		dev [mm]		rms [mm]		$D_2 > 0.5$ mm		$D_2 > 1$ mm		...
	P_1	P_2	P_1	P_2	P_1	P_2	P_1	P_2	P_1	P_2	
0.00	1.517	1.073	1.341	0.975	2.025	1.450	76.87 %	66.98 %	56.19 %	38.84 %	...
0.01	1.517		1.340		2.024		76.86 %		56.18 %		...
⋮	⋮		⋮		⋮		⋮		⋮		⋮
0.10	1.514	1.089	1.339	0.991	2.021	1.472	76.82 %	66.99 %	56.12 %	39.36 %	...
⋮	⋮		⋮		⋮		⋮		⋮		⋮
0.20	1.513	1.107	1.338	1.011	2.020	1.499	76.81 %	67.49 %	56.07 %	39.75 %	...
⋮	⋮		⋮		⋮		⋮		⋮		⋮
0.30	1.509	1.130	1.336	1.035	2.016	1.532	76.87 %	67.76 %	56.19 %	40.28 %	...
⋮	⋮		⋮		⋮		⋮		⋮		⋮
0.40	1.506	1.158	1.336	1.063	2.013	1.571	76.76 %	68.02 %	55.85 %	40.95 %	...
⋮	⋮		⋮		⋮		⋮		⋮		⋮
0.43	1.506		1.336		2.013		76.76 %		55.87 %		...
0.44	1.506		1.336		2.013		76.73 %		55.84 %		...
0.45	1.507	1.164	1.336	1.071	2.014	1.618	76.73 %	68.56 %	55.77 %	41.43 %	...
0.46	1.507		1.337		2.015		76.69 %		55.77 %		...
0.47	1.509		1.339		2.018		76.69 %		55.80 %		...
0.48	1.514		1.342		2.023		76.72 %		55.88 %		...
0.49	1.524		1.349		2.035		76.88 %		56.07 %		...

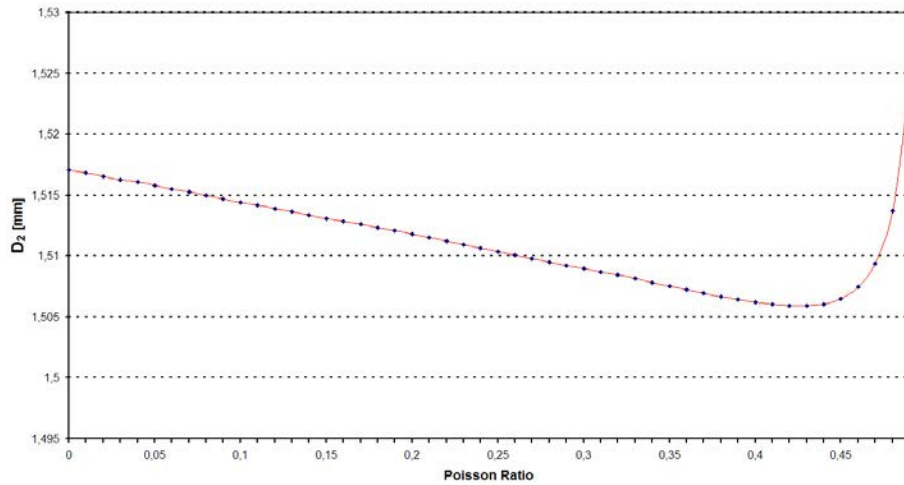


Fig. 6. Deviation between predicted and postoperative skin surface in dependence on POISSON's ratio ν for soft tissue with no significant volume change

The mean distance between simulated and postoperative skin surface of the entire head was 1.32 mm in one case and below 1 mm in the other case (1.5 mm or 1.1 mm respectively for the facial skin only), with a standard deviation in the same order and a median value of 1.15 mm or 0.79 mm respectively. For more than 50% of the entire skin surface (44% of the face) in one case, and more than 70% (60%) in the second case, the prediction error was below 1 mm , and for almost 80% (75%) and 90% (85%) below 2 mm . 10% (12%) and 3% (5%) of the surfaces show a deviation larger than 3 mm (Fig. 7).

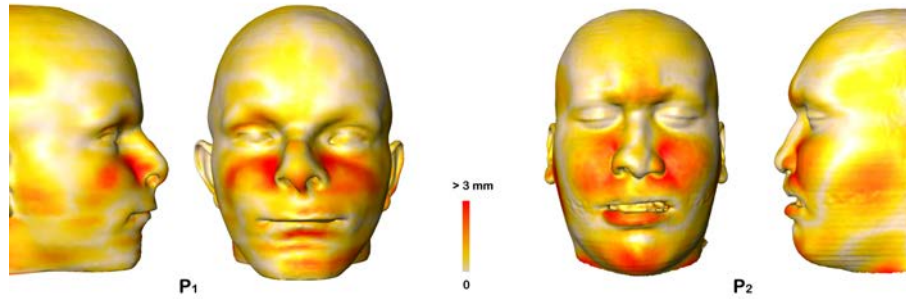


Fig. 7. Color coded deviation between prediction and postoperative result for an isotropic, homogeneous linear elastic tissue model

In a second study we investigated an *inhomogeneous* tissue model. Theoretically, for each tetrahedron appropriate histomechanic parameters have to be assigned. Therefore, a relationship between HOUNSFIELD values and mechanical properties is needed. To our knowledge such a relationship isn't available yet, and the determination of appropriate values for different tissue types is subject of ongoing research in biomechanics and elastography. In the literature we found some values, that are derived from experiments (Tab. 2). For a first parameter study we differentiated between muscle and embedding tissue, since muscle can easily be segmented within a range of $[-30, 100]$ HU.

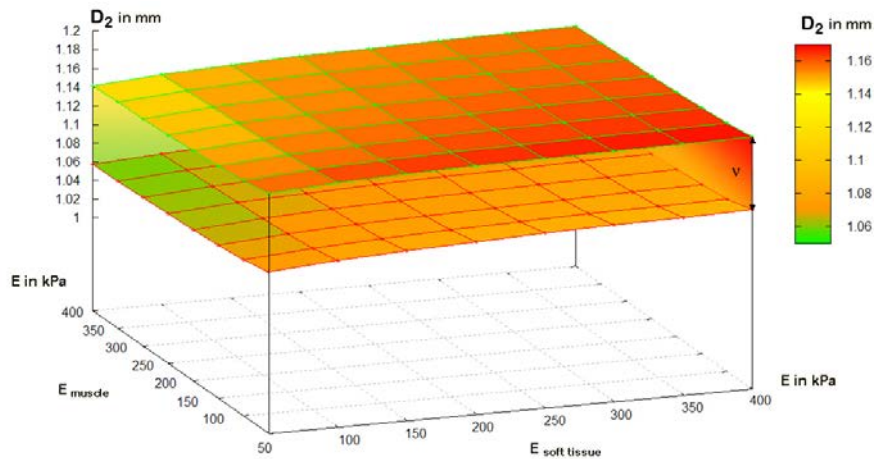
Table 2. Elastic properties of soft tissues, YOUNG's modulus E ($1\text{ Pa} = 1\text{ N/m}^2$)

Source	Skin [MPa]	Soft Tissue [kPa]	Fat [kPa]	Muscle [kPa]
Reihnsner, 1989 [13]	4...15	–	–	300
Holzapfel, 2000 [14]	0,1...2...	–	–	–
Elden, 1973 [15]	3,43...157	–	–	–
Azar, 2001 [16]	–	–	4,5...120	–
Duck, 1991 [11]	–	–	–	6,2...300
Maass, 1999 [17]	–	–	20...60	15...264
Krouskop, 1998 [18]	–	6,8...110	20	–
Ophir, 1999 [19]	–	–	20	–
Levinson, 1995 [20]	–	–	–	50...150

Table 3. Parameter study for patient 2: Mean prediction error for an *inhomogeneous* tissue model with varying POISSON ratios and elastic moduli

D_2	E_m	50 000				100 000				...	450 000			
		v_m	0.00	0.05	...	0.45	0.00	0.05	...		0.45	...	0.00	0.05
E_s	v_s													
50 000	0.00	1.073	1.075		1.088	1.067	1.070		1.084		1.057	1.059		1.073
	0.05	1.086	1.089		1.102	1.080	1.083		1.097		1.069	1.071		1.086
	⋮													
	0.45	1.144	1.146		1.158	1.137	1.140		1.153		1.124	1.127		1.141
100 000	0.00	1.079	1.081		1.091	1.073	1.075		1.088		1.062	1.064		1.079
	0.05	1.093	1.095		1.106	1.086	1.089		1.102		1.074	1.077		1.092
	⋮													
	0.45	1.150	1.151		1.162	1.144	1.146		1.158		1.130	1.133		1.147
⋮	⋮													
450 000	0.00	1.092	1.093		1.099	1.085	1.087		1.095		1.072	1.075		1.088
	0.05	1.107	1.108		1.114	1.099	1.101		1.109		1.086	1.088		1.102
	⋮													
	0.45	1.164	1.165		1.171	1.157	1.159		1.166		1.144	1.146		1.158

In order to keep the initial unstructured soft tissue grid for comparison, we relabeled the tissue elements (tetrahedra) according to the mean HOUNSFIELD values, using a barycentric sampling with selectable refinement. The resulting tissue grid then consists of two different tissue types that can be assigned individual values for v and E . In a first study for each tissue POISSON's ratio v was varied within the range of $[0 \dots 0.5[$, and YOUNG's modulus E within $[50 \dots 450]$ kPa (Tab. 3). For each combination an FE simulation of the tissue deformation has been conducted in the same way as for the homogeneous model. The deviation between the resulting skin surface and the postoperative result was again measured via the two-sided HAUSDORFF distance $D_2(v_s, E_s, v_m, E_m)$.

**Fig. 8.** Prediction quality of an inhomogeneous tissue model in dependence on YOUNG's moduli E and POISSON ratios v

Starting with a coarse increment, the limits of the simulation have been determined, to avoid unnecessary computation. All results are lying in-between the two colored planes, being depicted in Fig. 8. These two planes border all combinations of ν_s and ν_m within the given range $[0 \dots 0.5]$. The mean deviation between prediction and true postoperative outcome varies in dependence of the elastic moduli between 1 and 1.2 mm. Independent of the choice of POISSON's ratio, an optimum was found for YOUNG's modulus $E_m > 300$ kPa for muscle and $E_s < 100$ kPa for fatty or connective tissue. In a second run the tissue deformation has been computed with optimally chosen POISSON ratios, varying the elastic moduli within the range of $]0, 500]$ kPa at a higher resolution (Fig. 9).

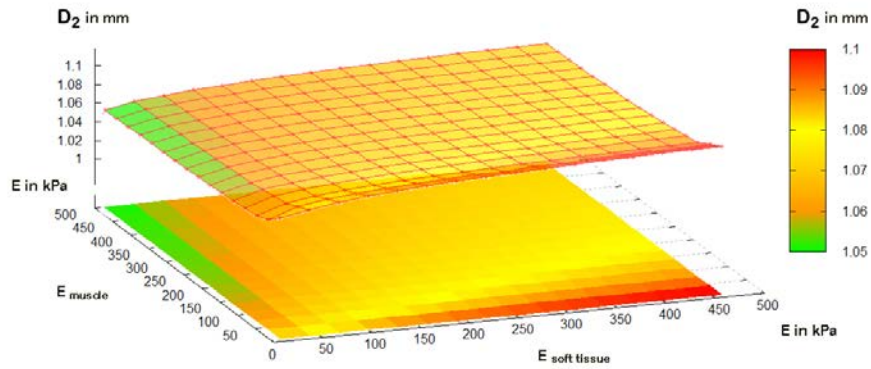


Fig. 9. prediction quality of an inhomogeneous tissue model in dependence on YOUNG's modulus E , with optimally chosen POISSON ratio ν

4 Results and Discussion

Although the resulting variation was only small in comparison to the homogeneous tissue model, the inhomogeneous model performed slightly better (Fig. 6 b). The best correspondence was found with $0.43 < \nu_m < 0.45$ and $E_m > 300$ kPa for muscle as well as with $0.44 < \nu_s < 0.47$ and $E_s < 50$ kPa for the embedding tissue. In contrast to our first investigation [7], the analysis of a second data set lead to a more plausible result, since the soft tissue volume remained almost constant. However, the net improvement of using inhomogeneous tissue models, or of fine tuning the elastic parameters does not significantly influence the prediction quality. These values rather have an effect on inner regions of high strains, that are typically located at the bone-tissue boundary. Other sources of error, like motion artifacts, reconstruction problems due to tightly closed lips and swelling are prevailing in our quantitative evaluation. Despite these factors and from a surgical point of view, a mean prediction error of 1 to 1.5 mm is quite acceptable for the assessment of bone relocations with regard to the aesthetic outcome. Two other pre- and postoperative data sets are available and will help us to further improve our volumetric modeling approach.

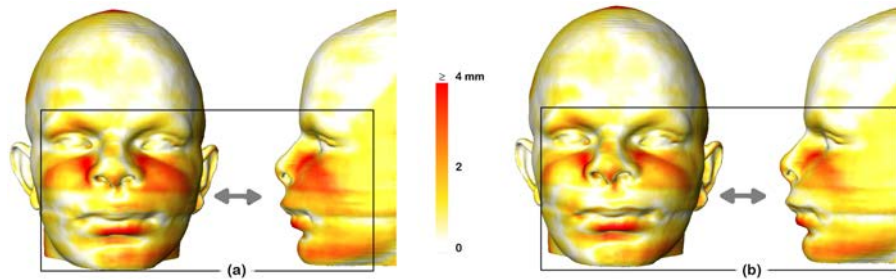


Fig. 10. Difference between soft tissue prediction and true postoperative outcome: a) using a homogeneous, and b) an inhomogeneous tissue model

A too coarse discretization of the tissue volume in combination with linear elements lead to an increasing approximation error, too. Instead of using higher order elements or choosing a discretization that is too fine, adaptive refinement techniques based on local error estimators can be used [21]. In Fig. 11 such a refinement is shown in the cheek regions where higher strains occur at the bony ridges. However, the improvements are very localized, and in view of long term tissue remodeling processes rather neglectable.

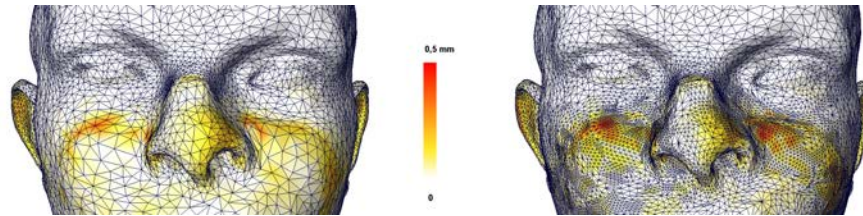


Fig. 11. difference between linear elements and adaptive refinement

The simulation results in general are already helpful for surgery planning. More pre- and postoperative data sets are to be compared for validation. A prospective study is targeted, to postoperatively investigate tissue deformation. Skin surface data are to be acquired for a period of 12 months after surgery, either with MRI or with surface digitizers. Thus, skin surface development can be recorded and quantified.

5 Acknowledgements

This work has been partially funded by the DFN, CoDiSP project (*Collaborative Distributed Surgery Planning*). We are very grateful to Prof. Klöppel, head of the *Klinik und Poliklinik für Diagnostische Radiologie, Universitätsklinikum Leipzig* for kindly providing us with pre- and postoperative CT data. Furthermore we would like to acknowledge that the 3D planning environment is based on the software Amira [22].

References

1. Landes CA, Zachar R, Diehl T, and Kovács AF: *Introduction of a three-dimensional anthropometry of the viscerocranium. Part II: Evaluating osseous and soft tissue changes following orthognatic surgery*. J Craniomaxillofac Surg 30, pp. 25–34 (2002)
2. Ayache N and Delingette H (eds.): *Surgery Simulation and Soft Tissue Modeling*, Lecture Notes in Computer Science, no. 2673, Springer-Verlag, Tokyo · Berlin · Heidelberg (2003)
3. Cotin S and Metaxas D (eds.): *Medical Simulation*, Lecture Notes in Computer Science, no. 3078, Springer-Verlag, Tokyo · Berlin · Heidelberg (2004)
4. Hierl T and Hemprich A: *A novel modular retention system for midfacial distraction osteogenesis*. Br. J. Oral Maxillofac Surg 38, pp. 623–626 (2000)
5. Zachow S, Gladilin E, Hege HC, and Deuffhard P: *Finite-element simulation of soft tissue deformation*. In: Proc. CARS 2000, pp. 23–28 (2000)
6. Zachow S, Gladilin E, Sader R, and Zeilhofer HF: *Draw & Cut: Intuitive 3D Osteotomy planning on polygonal bone models*. In: Proc. CARS 2003, pp. 362–369 (2003)
7. Zachow S, Hierl Th and Erdmann B: *On the predictability of tissue changes for osteotomy planning in maxillofacial surgery: A comparison with postoperative results*. In: Proc. CARS 2004, pp. 648–653 (2004)
8. Klöppel R, Hierl Th, Gosch D, et al.: *Kallusdistraction des Mittelgesichts: Anforderungen an die bildgebende Diagnostik*. Radiologie 39, pp. 1068–1078 (1999)
9. Besl PJ and McKay ND: *A method for registration of 3D shapes*. IEEE Trans. on Pattern Analysis and Machine Intelligence 14(2), pp. 239–256 (1992)
10. Aspert N, Santa-Cruz D, and Ebrahimi T: *MESH: Measuring errors between surfaces using the HAUSDORFF distance*. In: Proc. IEEE ICME, vol. 1, pp. 705–708 (2002)
11. Duck FA: *Physical Properties of Tissue – A Comprehensive Reference Book*. Academic Press, chap. 5, pp. 137 ff. (1991)
12. Fung YC: *Biomechanics: Mechanical Properties of Living Tissues*. 2nd edition, Springer (1993)
13. Reihnsner R: *Biomechanische Eigenschaften des kollagenen Bindegewebes*. In: *Das kollagene Bindegewebe: Symposium*, Mallinger R and Neumüller J (eds.), Wien (1988), pp. 30–41
14. Holzapfel GH: *Biomechanics of soft tissue*. In: *Handbook of Material Behaviour: Nonlinear Models and Properties*, Lemaitre J and Cachan LMT (eds.), Academic Press Inc., No. 7 in Biomech Reprint Series, pp. 1–12 (2000)
15. Elden HR (ed.): *Biophysical Properties of the Skin*. Interscience, John Wiley and Sons, Inc., New York (1973)
16. Azar FS, Metaxas DN, and Schnall MD: *A deformable finite element model of the breast for predicting mechanical deformations under external perturbations*. In: Proc. of the Int. workshop on deformable modeling and soft tissue simulation (2001)
17. Maaß H: *Untersuchung einer Methode zur nichtinvasiven Messung von Steifigkeitskoeffizienten an lebendem Gewebe mit multimodalen bildgebenden Verfahren*. Dissert. Fak. Maschinenbau, Universität Fridericiana zu Karlsruhe (1999)
18. Krouskop TA, Wheeler TM, Kallel F, Garra BS, et al.: *Elastic moduli of breast and prostate tissues under compression*. Ultrasonic Imaging 20, pp. 260–274 (1998)
19. Ophir J, Alam SK, Garra B, Kallel F, et al.: *Elastography: Ultrasonic estimation and imaging of the elastic properties of tissues*. Journal of Eng. in Medicine 213(3), pp. 203–233 (1999)
20. Levinson SF, Shinagawa M, and Sato T: *Sonoelastic determination of human skeletal muscle elasticity*. Journal for Biomechanics 28(10), pp. 1145–1154 (1995)
21. Deuffhard P, Leinen P and Yserentant H: *Concepts of an adaptive hierarchical finite element code*. IMPACT Comp. Sci. Eng. 1, pp. 3–35 (1989)
22. Stalling D, Westerhoff M, Hege, HC, et al.: *Amira - An Advanced 3D Visualization and Modeling System*, URL: <http://www.amiravis.com>